The Cryosphere Discuss., 7, 5823–5851, 2013
www.the-cryosphere-discuss.net/7/5823/2013/
doi:10.5194/tcd-7-5823-2013

The Cryosphere
Discussions
Open Access

Importance of basal processes in simulations of a surging Svalbard outlet glacier

R. Gladstone[1,2,3], M. Schäfer[1], T. Zwinger[4], Y. Gong[1], T. Strozzi[5], J. Moore[1,6,7], R. Mottram[8], and F. Boberg[8]

[1]Arctic Centre, University of Lapland, Rovaniemi, Finland
[2]VAW, Eidgenossische Technische Hochschule Zürich, ETHZ, Switzerland
[3]Antarctic Climate and Ecosystems Cooperative Research Centre, University of Tasmania, Hobart, Tasmania, Australia
[4]CSC – IT Center for Science Ltd., Espoo, Finland
[5]Gamma Remote Sensing and Consulting AG, Gümligen, Switzerland
[6]Department of Earth Sciences, Uppsala University, Uppsala, Sweden
[7]College of Global Change and Earth System Science & State Key Laboratory of Remote Sensing Science, Beijing Normal University, Beijing, China
[8]Danish Meteorological Institute, Copenhagen, Denmark

Received: 8 November 2013 – Accepted: 19 November 2013 – Published: 9 December 2013

Correspondence to: R. Gladstone (rupertgladstone1972@gmail.com)

Published by Copernicus Publications on behalf of the European Geosciences Union.

Abstract

The outlet glacier of Basin 3 (B3) of Austfonna icecap, Svalbard, is one of the fastest outlet glaciers in Svalbard, and shows dramatic changes since 1995. In addition to previously observed seasonal summer speed up associated with the melt season, the winter speed of B3 has accelerated approximately five fold since 1995. We use the Elmer/Ice full Stokes model for ice dynamics to infer spatial distributions of basal drag for the winter seasons of 1995, 2008 and 2011. This "inverse" method is based on minimising discrepancy between modelled and observed surface velocities, using satellite remotely sensed velocity fields. We generate steady state temperature distributions for the three time periods. Frictional heating caused by basal sliding contributes significantly to basal temperatures of the B3 outlet glacier, which exhibits a uniform steady state basal temperature at pressure melting point in all three cases.

We present a sensitivity experiment consisting of transient simulations under present day forcing to demonstrate that using a temporally fixed basal drag field obtained through inversion can lead to thickness change errors of the order of 2 m per year. Hence it is essential to incorporate the evolution of basal processes in future projections of the basin. Informed by a combination of our inverse method results and previous studies, we hypothesize a system of processes and feedbacks involving till deformation and basal hydrology to explain both the seasonal accelerations and the ongoing inter-annual speed up, and speculate on the wider relevance of deformable till mechanics to non-surging glaciers.

1 Introduction

Austfonna (ASF) is a large (approx. 8000 km^2) icecap in the Svalbard Archipeligo. ASF is divided into a number of drainage basins, one of which, basin 3 (B3), has recently been observed to accelerate (Dunse et al., 2012). Speculation on the dynamics of B3 extends back to the 19th century. Dowdeswell et al. (1999) reviewed evidence on the

Discussion Paper | Discussion Paper | Discussion Paper | Discussion Paper |

dynamics of B3 back to the 19th century. Presence of heavy crevassing was taken to indicate fast flow in the 1870s (Nordenskiold, 1875), whereas relatively smooth surface topography is thought to indicate stagnation in the 1980s (Dowdeswell et al., 1999). SAR interferometry in the early 1990s shows flow speeds in 1992 and 1994, of up to 90 $\mathrm{m\,a^{-1}}$ and 50 $\mathrm{m\,a^{-1}}$ respectively over a transect approx. 7.5 km upstream from the ocean margin (Dowdeswell et al., 1999). Ice velocity was of comparable magnitude in 1995 (Dunse et al., 2012) but has recently accelerated to give winter velocities up to 200 $\mathrm{m\,a^{-1}}$ at similar locations as the 1992 and 1994 observations, and a velocity range (due a strong seaonal cycle) near the margin of 300–700 $\mathrm{m\,a^{-1}}$ (Dunse et al., 2012). In the current study we use an ice dynamic computer model to make inferences about basal properties and processes of B3 using recent satellite observations, and focus on the winter velocity increase rather than the seasonal cycle.

The fast flow of B3 is certainly due to basal sliding; ice deformation rarely accounts for more than 5 $\mathrm{m\,a^{-1}}$ over Austfonna (Dowdeswell et al., 1999). This means that a purely ice dynamic model is not sufficient to simulate the velocity evolution of B3; some representation of the changing basal processes, which permit an increase in sliding, must be included.

A note on terminology: We use the term “sliding” to mean motion of the base of the glacier, irrespective of whether this is due to sliding of the glacier over its bed or deformation of underlying sediment. In the absence of a universally accepted definition of the term “surge” as applied to a glacier or ice stream, we utilise our own definition. By “surge-type” glacier we mean a coupled glacier-bed system showing strong (factor three or more) variability of ice velocity with a cyclic nature, independent of changes in external forcing (such as surface mass balance or temperature). By “surge” we mean the fast flowing phase of a surge-type glacier during which the glacier shows rapid and sustained acceleration. We note that, by this fairly generic definition, different underlying mechanisms can lead to surge-type glaciers with a large range of periodicities and magnitudes.

TCD
7, 5823–5851, 2013

Title Page
Abstract | Introduction
Conclusions | References
Tables | Figures
◀◀ | ▶▶
◀ | ▶
Back | Close
Full Screen / Esc
Printer-friendly Version
Interactive Discussion

Svalbard glaciers are known to be commonly (Jiskoot et al., 2000), or perhaps overwhelmingly, surge-type (Lefauconnier and Hagen, 1991; Sund et al., 2009). A Svalbard surge-type glacier typically spends several decades to a few centuries in a quiescent state, then becomes active for periods as long as a decade Dowdeswell et al. (1991). The surge phase for Svalbard glaciers is significantly longer than for surging glaciers in other regions Dowdeswell et al. (1991), however the relative increase of velocity during a surge is relatively lower than for glaciers in other regions. The longest surge phase listed by Dowdeswell et al. (1991) was for Bodleybreen on Vestfonna ice cap which lasted for between 5 and 13 yr, with a best estimate of 7 yr. Surge speeds in Svalbard glaciers are typically many times greater than the stagnant phase since sliding becomes the dominant factor of ice flow. The speed of the B3 glacier in 1995 was much faster than the typical stagnant quiescent state of Svalbard glaciers which do not slide, and given the continued or accelerating velocity, suggests that the glacier has been in a fast flowing or surging state for perhaps 20 yr, with an even faster state for the past few years. Given that B3 surface morphology indicated stagnant conditions most recently during in the 1980s, the B3 basin may be experiencing an extremely long-lasting surge, or variations in fast-flowing glacier, or it may be an acceleration into a fast flow regime that is not part of cyclic behaviour. in this respect B3 may be behaving more like an Antarctic ice stream where long-period slow down and speed-up events occur likely driven by changes in basal hydrology or "water piracy" (Tulaczyk et al., 2000; Anandakrishnan and Alley, 1997; Bougamont et al., 2011).

Svalbard surge-type glaciers are thought to be most commonly underlain by fine-grained and potentially deformable beds (Jiskoot et al., 2000). Although the importance of deformable sediment beneath glaciers was already widely discussed in the literature of the 1980s (Boulton and Hindmarsh, 1987; Clarke, 1987a), ice dynamic modelling studies have only recently begun to simulate till deformation. Vieli and Gudmundsson (2010) model the till as an incompressible non-linear viscous medium and do not consider the effects of hydrology. However, Iverson (2010) shows that sediment typically

TCD
7, 5823–5851, 2013

deforms plastically and that the yield stress is strongly dependant on effective pressure, which in turn is strongly dependant on water pressure and therefore also on hydrology.

Further modelling studies have investigated the impact of water content in deformable sediment on ice dynamics. Bougamont et al. (2011) solved a first order differential equation for evolution of porosity in the till, and showed that, with a plastic bed model and a simple parameterisation for basal water availability, low frequency oscillations could be obtained (of the order of 10^3 yr) in an idealised ice sheet. Van Pelt and Oerlemans (2012) used a simple diffusion relation to simulate evolution of till water content and were able to demonstrate, for a plastic till (some of their simulations also included a small linearly viscous component), both low frequency oscillations (driven by changes in temperature distribution) and high frequency oscillations (driven by changes in till water distribution) in an idealised outlet glacier, with till strength being an important factor governing possible oscillatory behaviour. van der Wel et al. (2013) used a plastic till model with a hydrology model that incorporates representation of channelised flow at the ice–till interface to demonstrate the important control connectivity through to the grounding line has on upstream sliding.

These till studies all express yield stress as a function of one unknown, imposing dependency between effective pressure and porosity. Clarke (1987b) provides a physical framework based on soil studies in which both positive and negative dilatancy can occur, and the evolution of yield stress is a function of both porosity and effective pressure as independent variables.

Simulations incorporating plastic till deformation have not yet been applied to B3. However, Dunse et al. (2011) simulated cyclic behaviour on B3 using a basal drag formulation dependant on temperature and overburden pressure. Till water is not explicitly simulated by Dunse et al. (2011), but may be implicit in the temperature dependency.

The current study does not attempt to simulate evolution of till properties, but instead uses inverse and transient simulations with an ice dynamic model to make inferences about key physical processes, which will in turn guide till model development. Section 2 presents a time series of three winter season inverse simulations whereby basal stress is derived to optimise the fit of simulated surface velocities to observations. Section 3 presents transient simulations as a sensitivity experiment to quantify the importance of omitting evolution of basal stress. Section 4 discusses possible feedback mechanisms to explain the acceleration of B3 in light of the new simulations.

1.1 Open source tools

A number of open source software projects made possible the inverse modelling and other analyses in the current study. Elmer/Ice (Gagliardini et al., 2013) was used for ice dynamic simulations. Mesh generation for the simulations used YAMS (http://www.ann.jussieu.fr/frey/publications/RT-0252.pdf) and GMSH (Geuzaine and Remacle, 2009). Analyses and presentation of outputs utilised Paraview (Ahrens et al., 2005).

2 Inverse modelling

Modelling results presented in the current study were obtained using the Elmer/Ice full stokes model for ice dynamics (Gagliardini et al., 2013). In this section, we present inverse simulations using the method of Arthern and Gudmundsson (2010) as implemented in Elmer/Ice by Gillet-Chaulet et al. (2012). The experimental setup is the same as that used for neighbouring Vestfonna icecap (Schäfer et al., 2013), following the work of Schäfer et al. (2012), except where stated otherwise.

2.1 Model setup

The approach to inverse modelling involves optimisation of the basal drag coefficient, C, to provide a best fit between observed and simulated surface velocities. C is given by

$$\tau_b = C u_b \tag{1}$$

where τ_b is basal shear stress and u_b is basal ice velocity.

TCD
7, 5823–5851, 2013

A three-step process is followed: the inversion is carried out with a uniform (−7 °C) temperature distribution; a steady-state temperature simulation is carried out using the velocities derived from the inversion; finally the inversion is repeated using the derived steady state temperatures. This gives consistent temperature and velocity fields. The geometry is kept fixed at all stages. In some cases further temperature – inversion iterations were carried out, but these showed little or no further change. The steady state temperature simulation incorporates deformational heating and heating due to friction at the bed, as described by Schäfer et al. (2013).

The steady-state temperature simulation is carried out with a fixed temperature boundary condition at the upper surface

$$T_s = -7.684 - 0.004z \tag{2}$$

where T_s is surface ice temperature, z is height a.s.l., and the constant values on the right hand side represent sea level temperature (in °C) and lapse rate (in °C m^{-1}) respectively, with values as in Schäfer et al. (2013).

A heat flux, Q_b, boundary condition is used at the base of the ice

$$Q_b = 0.063 + u_b \tau_b \tag{3}$$

where the terms on the right hand side are geothermal heat flux (in $W m^{-2}$), as in Schäfer et al. (2012), and frictional heat flux respectively.

The ice geometry (surface elevation and bedrock heights) are based on Norwegian Polar Institute maps and various ice thickness data as described in Sect. 3.3 of Dunse et al. (2011).

2.1.1 Observed velocities

Ice surface velocities based on satellite remote sensing are used. Velocities were obtained using interferometry for the period December 1995 to January 1996 (henceforth “1995 velocities”), offset tracking for the period January to March 2008 (henceforth

TCD
7, 5823–5851, 2013
Surging Svalbard glacier
R. Gladstone et al.

“2008 velocities”), and a combined interferometry/tracking approach (effectively offset-tracking over B3) for the period March to April 2011 (henceforth “2011 velocities”). A more detailed description is given by (Schäfer et al., 2013). It is important to emphasize that all these observations indicate velocities prior to the melt-season speed up (Dunse et al., 2012).

The 1995 data set of observed surface velocities, based on interferometry, is smooth and has good coverage (Dowdeswell et al., 2008). The 2008 and 2011 data sets contain many data gaps and regions with noisy error fields (Fig. 1), but the dramatic speed up of the B3 outlet glacier is clearly visible.

Since we wish to simulate the basal properties of B3 over time we need to provide a smooth input field for the inverse modelling. Therefore the following processing of the noisy velocity fields took place. The 2008 and 2011 velocities were smoothed using an 11 point (approx. 3 km) conic filter. The B3 outlet glacier region from 2008 and 2011 was then copied over to the 1995 velocity field and smoothed using interpolation over a buffer zone, so that the smooth and complete 1995 dataset can be used where data are missing or contain too much high amplitude noise to be useful. This results in three data sets for inverse modelling, using 1995 velocities for regions other than B3, but with the 1995, 2008 and 2011 velocities respectively for the B3 region (Fig. 2).

2.1.2 Mesh generation

For consistency, all simulations in the current study use the same mesh (Fig. 3). The mesh is unstructured in the horizontal, and extruded in the vertical with 10 equally spaced layers. The horizontal mesh resolution varies between approximately 250 m and 2.5 km. Mesh refinement is guided by 1995 velocity magnitude (smaller element size for higher velocities), except for B3. Mesh refinement for B3 is based on 2011 velocities with additional resolution enhancement.

Previous studies (Schäfer et al., 2013; Gillet-Chaulet et al., 2012) have implemented mesh refinement based on the Hessian of the velocity field in order to give a spatially uniform truncation error. Such an approach was not chosen for the current study due to the motivation to simulate greatly differing observed velocity fields on the same mesh, and to carry out transient simulations in which the velocity field is allowed to evolve.

2.2 Inverse modelling results

The simulated surface velocities for all three time periods show (unsurprisingly given the inverse approach) a good match to observations. The 2011 simulated velocity field is shown with the model mesh and the icecap surface in Fig. 3. We mainly present results from the 1995 and 2011 simulations, with 2008 providing a less significant intermediate state.

The basal drag coefficient β is shown in Fig. 4 for the 1995 and 2011 simulations. Basal sliding accounts for most of the surface velocity. The 2011 β distribution shows, in comparison to the 1995 β, both a reduction in the minimum value of β, and an increase in the area of low β corresponding to the increase in area of fast flow.

We compare the gravitational driving stress, τ_D, with the basal shear stress, τ_b, in Fig. 5. τ_b is given by Eq. (1) and is dependant on the surface velocity observations, basal drag law, ice geometry and on shear stresses in the ice model. τ_D is a function of the icecap geometry only, and is given by

$$\tau_D = \rho g H \nabla(s), \tag{4}$$

where ρ is ice density ($910\,\mathrm{kg\,m^{-3}}$), g is gravitational acceleration ($9.81\,\mathrm{m\,s^{-2}}$), H is ice thickness and $\nabla(s)$ is the ice surface gradient.

In 1995 τ_D is approximately 10 to 20 kPa higher than τ_b in the fast flowing B3 outlet glacier, and is approximately the same amount lower than τ_b at or just beyond the shear margins. This suggests that even in 1995 the bed strength is insufficient to balance the driving stress, and support from the lateral margins compensates. In 2011 the pattern is the same but stronger, with τ_b dropping close to zero and $\tau_D - \tau_b$ around 50 kPa. The imbalance also occurs over a larger area (corresponding to the increased region of fast flow).

TCD
7, 5823–5851, 2013

Note that τ_D is calculated using the same ice cap geometry for different time periods. To test sensitivity of τ_D to the evolving ice cap free surface we calculated τ_D also using the ice sheet geometry from the transient 2011β simulation (Sect. 3). The results (not shown) show very little difference to Fig. 5, because it is the change in τ_b that dominates rather than the change in τ_D.

3 Forward modelling

Further simulations are carried out to investigate sensitivities to thermodynamic terms and to basal processes.

3.1 Transient simulations

Two transient simulations of 100 yr were carried out to compare the evolution of B3 when the 2011 basal drag is used (henceforth experiment $T11$) against the use of the 1995 basal drag ($T95$). The aim is an experiment to investigate sensitivity of B3 evolution to basal drag; it is not a future prediction. Forcing is approximately present day.

Initial icecap geometry is as described in the setup for inverse modelling (Sect. 2). Temperature is given by the steady state temperature derived using the inverse method for 1995. This temperature field is used for both T95 and T11 experiments as we aim to isolate the impact of basal drag. Given that motion occurs primarily through sliding rather than deformation, temperature is held constant throughout the simulations.

Surface mass balance (smb) is given by HIRHAM5, a regional atmospheric climate model (Christensen et al., 2007). HIRHAM5 is based on a subset of the (Undén et al., 2002) and ECHAM models (Roeckner et al., 2003) combining the dynamics of the former model with the physical parameterization schemes of the latter. Bilinear interpolation is used to interpolate from the approx. 5 km resolution of HIRHAM to the finer

Discussion Paper | Discussion Paper | Discussion Paper | Discussion Paper |

TCD

7, 5823–5851, 2013

resolution Elmer mesh. The smb does not evolve through time; rather the 1990s mean smb is used.

Both simulations show changes in surface elevation over much of the icecap due to discrepancies between the divergence of the velocity field and the HIRHAM 1990s smb. The $T11$ simulation shows a large (up to $1.8\,\mathrm{m\,a^{-1}}$) relative surface lowering compared to $T95$ in the B3 interior (Fig. 6).

The $T11$ simulation shows a thickening near the margin during the first two decades relative to the $T95$ simulation due to the greater discharge from the interior.

3.2 Steady state simulations

As discussed in the Introduction, observations suggest a quiescent phase for B3 extending back in time up to a century from the 1980s, with the implication that the 1980s basal temperature may have been close to steady state, resulting from a long period of gradual thickening and near zero velocities. Here steady state simulations are carried out to investigate the sensitivity of steady state basal temperatures to geothermal heat flux, advection, and frictional heat generation at the bed.

A simulation with no advection terms (henceforth experiment SS for "steady state") was carried out as a proxy for 1980s basal temperatures. This simulation is repeated with geothermal heat flux, a poorly constrained parameter, halved from the value used in the T95 and t11 experiments to $31.5\,\mathrm{mW\,m^{-2}}$ (SSLG for "steady state low geothermal heat flux"). These two experiments are designed such that the resulting temperature distribution is determined mainly by vertical diffusion.

In addition to the steady state simulation with full thermodynamics using the 1995 simulated velocity and basal drag coefficient fields (SS95), an identical simulation with frictional heating removed is carried out (SS95NF). Note that SS95 is identical (except for initial conditions) to the second step of the inversion process, Sect. 2.

The basal temperatures resulting from all four simulations described above are shown in Fig. 7 and are discussed further in Sect. 4.

4 Discussion

We discuss possible mechanisms for surging and whether the simulations presented here support them. Key properties of basal processes of glacier systems and their interactions are shown in Fig. 8 (see also Introduction). An outlet glacier for which (a subset of) these processes are active may or may not exhibit cyclic (surge) behaviour. Generation of till material and evolution of the grain size distribution are not considered here but we include properties directly related to hydrology of both till and ice–till interface, and also effects of ice sheet geometry.

We consider which of these processes act to either restore or amplify a perturbation away from a steady state (or “attractor” in state space), in other words which processes act to return a glacier system towards steady state (negative feedbacks) or amplify the perturbation away from steady state (positive feedbacks). Note that in the context of internal periodicity, the “attractor” would likely be a hypothesized unstable steady state that lies within the periodic extremes. Any closed loop of processes in Fig. 8 indicates a feedback loop whose sign depends on the number of red arrows in the loop. Note that oscillations can arise from strongly non linear negative feedbacks, or from positive feedbacks with a limited temporal effect, or from combinations of positive and negative feedbacks.

Ice thickness – driving stress feedback. Ice thickening causes increased velocity due to increased driving stress. The combined increase in thickness and velocities increases the flux of ice discharged from the system, reducing ice thickness. This is a negative feedback, though it has previously been erroneously referred to as a positive feedback (Fowler et al., 2001).

Ice thickness – temperature feedback. Thicker ice insulates the bed and allows warmer steady state temperatures at the bed due to the warming effect of the geothermal heat flux. Warming at the bed increases the possibility of sliding, and the effective increase of heat generation at the bed potentially increases sliding velocity. This is a strongly non-linear (due to significance of the pressure melting point) long time scale (heat diffuses slowly through ice) negative feedback that will tend to speed up a thick outlet glacier or slow down a thin outlet glacier.

These two negative feedback loops alone would be expected to lead either to a steady state thickness profile in which smb is balanced by driving stress, or long time scale oscillations (order 10^3 a) due to thermoviscous instability (Boulton and Hindmarsh, 1987; Fowler et al., 2001; Van Pelt and Oerlemans, 2012).

Efficient drainage feedback. The relationship between basal water and sliding is complicated, but the first order response is an increase in sliding caused by increase in basal water. But increased basal water pressure also increases rate of discharge of water, reducing sliding. This is a highly non-linear negative feedback, with efficient drainage channels forming in response to high basal water content (Rothlisberger, 1972; Schoof, 2010). Such channels can drain basal water quickly, greatly reducing sliding velocities. Efficient drainage channels are typically considered to be a hard bed process, but if the timescale for water penetration of subglacial sediment is slow compared to the meltwater source (from in situ melting or penetration of surface melt) the process can also occur at the ice–till interface.

Friction heating. Friction due to either till deformation or sliding of ice over the bed causes heating and, where basal temperature is at the pressure melting point, increased melting, providing additional water to the till or ice–till interface. This decreases effective pressure, weakening till and enhancing flow speed (Iverson, 2010), providing a strong positive feedback.

Water/till strength feedbacks. The interactions between deformation and till properties are complex. As stated above, increased water pressure leads to reduced till yield strength, making deformation more likely. However, deformation can lead to either dilation (which weakens the till) or compression (which strengthens the till). Dilation is the expansion of consolidated till (and thus increase in porosity) in response to shearing. Dilatancy decreases with effective pressure and porosity (Clarke, 1987b). This is further complicated by water availability. If insufficient water is available then dilation can strengthen instead of weaken the till due to decreasing water pressure as porosity increases (Iverson, 2010). This network of dependencies is hard to resolve without a detailed model for till evolution.

We argue against a hard bedded sliding mechanism. B3 exhibits seasonal cyclicity in addition to the ongoing (inter-annual) speed up (Dunse et al., 2012). The only plausible mechanism for seasonality is due to surface meltwater reaching the bed and causing either basal sliding or till deformation. The reduction in velocity after the melt season can only be due to drainage of the excess basal water, most likely through efficient drainage channels. If both the seasonal speed up and the interannual acceleration are due to hard bedded sliding it is hard to explain why the additional water needed for the interannual acceleration is not discharged by the same method as the seasonal acceleration after the melt season. The possibility that seasonal acceleration occurs due to sliding near the ice cap margin whereas interannual acceleration occurs due to upstream water build up can be discounted due to the similar spatial patterns of both types of acceleration (Dunse et al., 2012).

We therefore hypothesize that the seasonal cycle is governed by the evolution of hydrology at the ice–till interface in response to penetration of surface melt, and that the interannual acceleration is governed by evolving by till properties, of which porosity, water pressure and permeability are perhaps the most important. This is consistent with previous studies that point to soft bed mechanisms for Svalbard glacier surges (Dowdeswell et al., 1999; Jiskoot et al., 2000; Murray et al., 2003). The physical separation of the seasonal and interannual accelerations could be due to the difference in timescales: seasonal melt events may be too short a timescale to permeate into the sediment and instead form drainage channels at the ice–till interface.

Reality may not be so simple: "sticky" spots (bedrock rises protruding through the sediment) may become important once τ_b has passed the yield stress.

The 2000s in Svalbard were historically very warm, likely warmer than any period in the previous 1000 yr (Grinsted et al., 2006; Virkkunen et al., 2007; Divine et al., 2011). Franklinbreen on Vestfonna is also presently undergoing a similar increase in velocity from 1995 to 2010 (Pohjola et al., 2011) as B3. This warm period may induce an earlier,

TCD
7, 5823–5851, 2013

Title Page
Abstract Introduction
Conclusions References
Tables Figures
◂ ▸
Back Close
Full Screen / Esc
Printer-friendly Version
Interactive Discussion

stronger or longer surge of B3 due to increased surface meltwater reaching the bed. Whether such warming could lead to a change in behaviour of B3 such as more rapid surge cycles, or even sustained fast flow, remains an open question.

4.1 Implications of modelling results

Given the likely situation that ASF overlies a plastically deformable till, we consider the significance of our basal stress calculations from the inverse simulations (Fig. 5). The relatively small and uniform excess of τ_D over τ_b in 1995 suggests that the till may already be starting to fail, but that τ_D is still close to the till yield stress, with the larger difference seen in 2011 suggesting widespread till failure. Given that changes in τ_D between 1995 and 2011 are relatively small (Sect. 2), this implies a reduction in the till yield strength, most likely caused by an increase in pore water pressure and or porosity (i.e. dilation) in the till. Pore water pressure increase is consistent with an increase in water production at the bed resulting from the friction heating feedback. An alternative explanation is that the till was overconsolidated in 1995 and the weakening is due to dilation. Likely both effects contribute.

The high spatial variability in modelled basal stress may be due to the presence of "sticky" spots, localised regions where bedrock protrudes through the sediment (Fowler et al., 2001). However, an equally likely explanation comprises the noisy error fields in observed velocities.

Simulated steady state basal temperature for ASF in the absence of advection (i.e. temperature distribution is driven by diffusion of geothermal heat through the ice) shows strong sensitivity to the geothermal heat flux, a poorly constrained parameter for ASF. Halving the chosen geothermal heat flux value of 0.063 $\mathrm{W\,m^{-2}}$ changes the steady state basal temperature distribution from widespread attainment of pressure melting point to cold bedded throughout ASF (Fig. 7 top panel).

This is consistent with the theory of the bed reaching pressure melting point due to gradual thickening as a trigger for the surge phase, but more accurate knowledge

TCD
7, 5823–5851, 2013

of the geothermal heat flux would be needed in order to assess how strongly these simulations support the theory.

While the region of basal melting due to geothermal heating could extend to the onset area for B3 fast flow (Fig. 7 top right), the advection of heat once sliding is initiated would tend to reduce the temperature below pressure melting point throughout the fast flow area (Fig. 7 bottom left). This not only emphasizes the importance of friction heating (Fig. 7 bottom right), but suggests a mechanism for accelerating surge shutdown: if shut down is due to refreezing at the bed as a result of thinning, the advection of heat away from the fast flow region (ultimately this heat is transported to the ocean) reduces the amount of thinning needed to refreeze the bed, shortening the surge duration.

5 Conclusions

We have conducted simulations to demonstrate that the assumption of a linear relationship between basal drag and basal velocity, along with a temporaly fixed coefficient, can lead to large errors in ice cap evolution.

The proposed soft bed surge mechanism of Fowler et al. (2001) is likely applicable to Austfonna's Basin 3, with the addition of a seasonal cycle arising from surface melt reaching the ice–till interface bed and then draining through efficient drainage channels, without ever penetrating significantly into the sediment.

Our simulations are consistent with this theory, and suggest in addition that the increase in advection of heat due to sliding is likely to shorten the surge phase of Basin 3. Observations and simulations are consistent with a quiescent phase ending in the 1990s, with rapid acceleration occuring the 2000s.

Arguments presented here, and in previous studies, point to the importance of incorporating basal processes into future ice sheet models for applications in which sliding may occur, and that both for hard bed and soft bed sliding hydrology is key. In particular, modelling the interaction between sediment properties and water pressure evolution is essential in order separate internal cyclicity from climatic forcing and to predict future behaviour of Austfonna.

Acknowledgements. We wish to thank Thorben Dunse from the University of Oslo for providing bedrock and surface elevation data. The satellite velocity data were produced with support of the EU FP6 INTEGRAL Project (1995), the ESA DUE GLOBGLACIER Project (2008) and the EU FP7 CRYOLAND Project (2011). We wish to thank Fabien Gillet-Chaulet from the Université Joseph Fourier for making available his code for the inverse modelling. We acknowledge CSC – IT Center for Science Ltd. for the allocation of computational resources. This work was performed at the Arctic Centre at the University of Lapland through funding by projects SVALI and SvalGlac. This publication is contribution number 31 of the Nordic Centre of Excellence SVALI, Stability and Variations of Arctic land Ice, funded by the Nordic Top-level Research Initiative.

References

Ahrens, J., Geveci, B., and Law, C.: 36 – ParaView: An End-User Tool for Large-Data Visualization, in: Visualization Handbook, edited by: Hansen, C. D., and Johnson, C. R., Butterworth-Heinemann, Burlington, 717 pp., LXXII, 2005. 5829

Anandakrishnan, S. and Alley, R.: Stagnation of ice stream C, West Antarctica by water piracy, Geophys. Res. Lett., 24, 265–268, doi:10.1029/96GL04016, 1997. 5827

Arthern, R. J. and Gudmundsson, G. H.: Initialization of ice-sheet forecasts viewed as an inverse Robin problem, J. Glaciol., 56, 527–533, 2010. 5829

Bougamont, M., Price, S., Christoffersen, P., and Payne, A. J.: Dynamic patterns of ice stream flow in a 3-D higher-order ice sheet model with plastic bed and simplified hydrology, J. Geophys. Res.-Ea. Surf., 116, F04018, doi:10.1029/2011JF002025, 2011. 5827, 5828

Boulton, G. and Hindmarsh, R.: Sediment deformation beneath glaciers – rheology and geological consequences, J. Geophys. Res.-Sol. Ea., 92, 9059–9082, doi:10.1029/JB092iB09p09059, 1987. 5827, 5836

Christensen, O., Drews, M., Christensen, J., Dethloff, K., Ketelsen, K., Hebestadt, I., and Rinke, A.: The HIRHAM regional climate model version 5 (β), Danish Meteorological Institute Technical Report 06-17, available at: http://www.dmi.dk/fileadmin/Rapporter/TR/tr06-17.pdf (last access: 2 December 2013), 2007. 5833

TCD
7, 5823–5851, 2013

Surging Svalbard glacier

R. Gladstone et al.

Clarke, G.: Fast glacier flow – ice streams, surging, and tidewater glaciers, J. Geophys. Res.-Sol. Ea., 92, 8835–8841, doi:10.1029/JB092iB09p08835, 1987a. 5827

Clarke, G.: Subglacial till – a physical framework for its properties and processes, J. Geophys. Res.-Sol. Ea., 92, 9023–9036, doi:10.1029/JB092iB09p09023, 1987b. 5828, 5836

Divine, D., Isaksson, E., Martma, T., Meijer, H. A. J., Moore, J., Pohjola, V., van de Wal, R. S. W., and Godtliebsen, F.: Thousand years of winter surface air temperature variations in Svalbard and northern Norway reconstructed from ice-core data, Polar Res., 30, 7379, doi:10.3402/polar.v30i0.7379, 2011. 5837

Dowdeswell, J., Hamilton, G., and Hagen, J.: The duration of the active phase on surge-type glaciers – contrasts between Svalbard and other regions, J. Glaciol., 37, 388–400, 1991. 5827

Dowdeswell, J., Unwin, B., Nuttall, A., and Wingham, D.: Velocity structure, flow instability and mass flux on a large Arctic ice cap from satellite radar interferometry, Earth Planet. Sc. Lett., 167, 131–140, doi:10.1016/S0012-821X(99)00034-5, 1999. 5825, 5826, 5837

Dowdeswell, J. A., Benham, T. J., Strozzi, T., and Hagen, J. O.: Iceberg calving flux and mass balance of the Austfonna ice cap on Nordaustlandet, Svalbard, J. Geophys. Res.-Ea. Surf., 113, F03022, doi:10.1029/2007JF000905, 2008. 5831

Dunse, T., Greve, R., Schuler, T. V., and Hagen, J. O.: Permanent fast flow versus cyclic surge behaviour: numerical simulations of the Austfonna ice cap, Svalbard, J. Glaciol., 57, 247–259, 2011. 5828, 5830

Dunse, T., Schuler, T. V., Hagen, J. O., and Reijmer, C. H.: Seasonal speed-up of two outlet glaciers of Austfonna, Svalbard, inferred from continuous GPS measurements, The Cryosphere, 6, 453–466, doi:10.5194/tc-6-453-2012, 2012. 5825, 5826, 5831, 5837

Fowler, A., Murray, T., and Ng, F.: Thermally controlled glacier surging, J. Glaciol., 47, 527–538, doi:10.3189/172756501781831792, 2001. 5835, 5836, 5838, 5839

Gagliardini, O., Zwinger, T., Gillet-Chaulet, F., Durand, G., Favier, L., de Fleurian, B., Greve, R., Malinen, M., Martín, C., Råback, P., Ruokolainen, J., Sacchettini, M., Schäfer, M., Seddik, H., and Thies, J.: Capabilities and performance of Elmer/Ice, a new-generation ice sheet model, Geosci. Model Dev., 6, 1299–1318, doi:10.5194/gmd-6-1299-2013, 2013. 5829

Geuzaine, C. and Remacle, J.-F.: Gmsh: A 3-D finite element mesh generator with built-in pre- and post-processing facilities, Int. J. Num. Meth. Eng., 79, 1309–1331, doi:10.1002/nme.2579, 2009. 5829

Gillet-Chaulet, F., Gagliardini, O., Seddik, H., Nodet, M., Durand, G., Ritz, C., Zwinger, T., Greve, R., and Vaughan, D. G.: Greenland ice sheet contribution to sea-level rise from a new-generation ice-sheet model, The Cryosphere, 6, 1561–1576, doi:10.5194/tc-6-1561-2012, 2012. 5829, 5831

Grinsted, A., Moore, J., Pohjola, V., Martma, T., and Isaksson, E.: Svalbard summer melting, continentality, and sea ice extent from the Lomonosovfonna ice core, J. Geophys. Res.-Atmos., 111, D07110, doi:10.1029/2005JD006494, 2006. 5837

Iverson, N. R.: Shear resistance and continuity of subglacial till: hydrology rules, J. Glaciol., 56, 1104–1114, 2010. 5827, 5836, 5837

Jiskoot, H., Murray, T., and Boyle, P.: Controls on the distribution of surge-type glaciers in Svalbard, J. Glaciol., 46, 412–422, doi:10.3189/172756500781833115, 2000. 5827, 5837

Leysinger Vieli, G. J.-M. C. and Gudmundsson, G. H.: A numerical study of glacier advance over deforming till, The Cryosphere, 4, 359–372, doi:10.5194/tc-4-359-2010, 2010. 5827

Lefauconnier, B. and Hagen, J.: Surging and calving glaciers in Eastern Svalbard, Norsk Polarinstitutt Meddelelser, Oslo, 1–130, 1991. 5827

Murray, T., Strozzi, T., Luckman, A., Jiskoot, H., and Christakos, P.: Is there a single surge mechanism? Contrasts in dynamics between glacier surges in Svalbard and other regions, J. Geophys. Res.-Sol. Ea., 108, 2237, doi:10.1029/2002JB001906, 2003. 5837

Nordenskiold, E.: Den Svenska Polarexpeditionen, 1872–73, Svenska Vetenskapsakademiets Handlingar 2, Stockholm, 1875. 5826

Pohjola, V. A., Christoffersen, P., Kolondra, L., Moore, J. C., Pettersson, R., Schafer, M., Strozzi, T., and Reijmer, C. H.: Spatial distribution and change in the surface ice-velocity field of Vestfonna ice cap, Nordaustlandet, Svalbard, 1995–2010 using geodetic and satellite interferometry data, Geografis. Ann. A, 93, 323–335, doi:10.1111/j.1468-0459.2011.00441.x, 2011. 5837

Roeckner, E., Bäuml, G., Bonaventura, L., Brokopf, R., Esch, M., Giorgetta, M., Hagemann, S., Kirchner, I., Kornblueh, L., Manzini, E., Rhodin, A., Schlese, U., Schulzweida, U., and Tompkins, A.: The atmospheric general circulation model ECHAM5. Part 1. Model description. Report no. 349, Max-Planck-Institut für Meteorologie (MPI-M), Hamburg, 2003. 5833

Rothlisberger, H.: Water pressure in intra and subglacial channels, J. Glaciol., 11, 177–203, 1972. 5836

Schoof, C.: Ice-sheet acceleration driven by melt supply variability, Nature, 468, 803–806, doi:10.1038/nature09618, 2010. 5836

Schäfer, M., Zwinger, T., Christoffersen, P., Gillet-Chaulet, F., Laakso, K., Pettersson, R., Pohjola, V. A., Strozzi, T., and Moore, J. C.: Sensitivity of basal conditions in an inverse model: Vestfonna ice cap, Nordaustlandet/Svalbard, The Cryosphere, 6, 771–783, doi:10.5194/tc-6-771-2012, 2012. 5829, 5830

Schäfer, M., Gillet-Chaulet, F., Gladstone, R., Pettersson, R., Pohjola, V. A., Strozzi, T., and Zwinger, T.: Assessment of heat sources on the control of fast flow of Vestfonna Ice Cap, Svalbard, The Cryosphere Discuss., 7, 5097–5145, doi:10.5194/tcd-7-5097-2013, 2013. 5829, 5830, 5831

Sund, M., Eiken, T., Hagen, J. O., and Kaab, A.: Svalbard surge dynamics derived from geometric changes, Ann. Glaciol., 50, 50–60, 2009. 5827

Tulaczyk, S., Kamb, W., and Engelhardt, H.: Basal mechanics of Ice Stream B, West Antarctica 1. Till mechanics, J. Geophys. Res.-Sol. Ea., 105, 463–481, doi:10.1029/1999JB900329, 2000. 5827

Undén, P., Rontu, L., Järvinen, H., Lynch, P., Calvo, J., Cats, G., Cuxart, J., Eerola, K., Fortelius, C., Garcia-Moya, J. A., Jones, C., Lenderlink, G., McDonald, A., McGrath, R., Navascues, B., Woetman Nielsen, N., Ådegaard, V., Rodrigues, E., Rummukainen, M., Rõõm, R., Sattler, K., Hansen Sass, B., Savijärvi, H., Wichers Schreur, B., Sigg, R., The, H., and Tijm, A.: HIRLAM-5 Scientific Documentation, available at: http://hirlam.org/index.php/hirlam-programme-53/general-model-description/synoptic-scale-hirlam (last access: 2 December 2013), 2002. 5833

van der Wel, N., Christoffersen, P., and Bougamont, M.: The influence of subglacial hydrology on the flow of Kamb Ice Stream, West Antarctica, J. Geopys. Res., 118, 97–110, doi:10.1029/2012JF002570, 2013. 5828

Van Pelt, W. J. J., and Oerlemans, J.: Numerical simulations of cyclic behaviour in the Parallel Ice Sheet Model (PISM), J. Glaciol., 58, 347–360, doi:10.3189/2012JoG11J217, 2012. 5828, 5836

Virkkunen, K., Moore, J. C., Isaksson, E., Pohjola, V., Peramaki, P., Grinsted, A., and Kekonen, T.: Warm summers and ion concentrations in snow: comparison of present day with Medieval Warm Epoch from snow pits and an ice core from Lomonosovfonna, Svalbard, J. Glaciol., 53, 623–634, doi:10.3189/002214307784409388, 2007. 5837

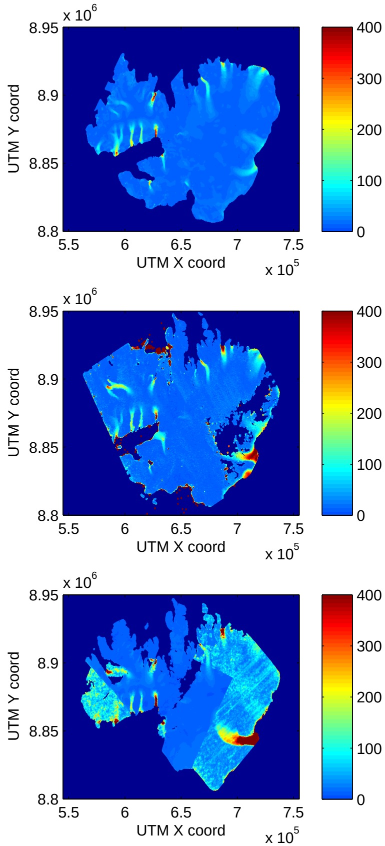

Fig. 1. Observed velocity magnitude (in $\mathrm{m\,a^{-1}}$) over Nordaustlandet from 1995 (top), 2008 (middle) and 2011 (bottom). B3 is the most prominent outlet glacier on the eastern side. Dark blue indicates no data. UTM zone is 33° N.

TCD
7, 5823–5851, 2013

Title Page
Abstract | Introduction
Conclusions | References
Tables | Figures
◂◂ | ▸▸
◂ | ▸
Back | Close
Full Screen / Esc
Printer-friendly Version
Interactive Discussion

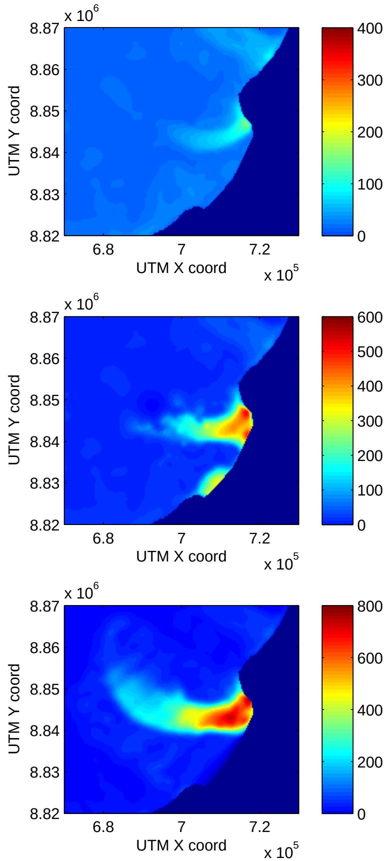

Fig. 2. Smoothed and patched (see main text for details) observed velocity magnitude (in $\mathrm{m\,a^{-1}}$) over B3, ASF from 1995 (top), 2008 (middle) and 2011 (bottom). Note the different colour scales. Dark blue indicates no data. UTM zone is 33° N.

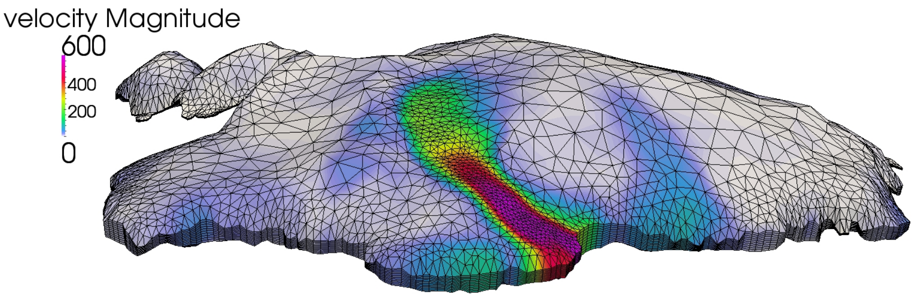

Fig. 3. Magnitude of the 2011 simulated surface velocity (in $\mathrm{m\,a^{-1}}$) on the refined ASF mesh showing B3 in the centre. Vertical exaggeration is 25.

TCD
7, 5823–5851, 2013
Surging Svalbard glacier
R. Gladstone et al.

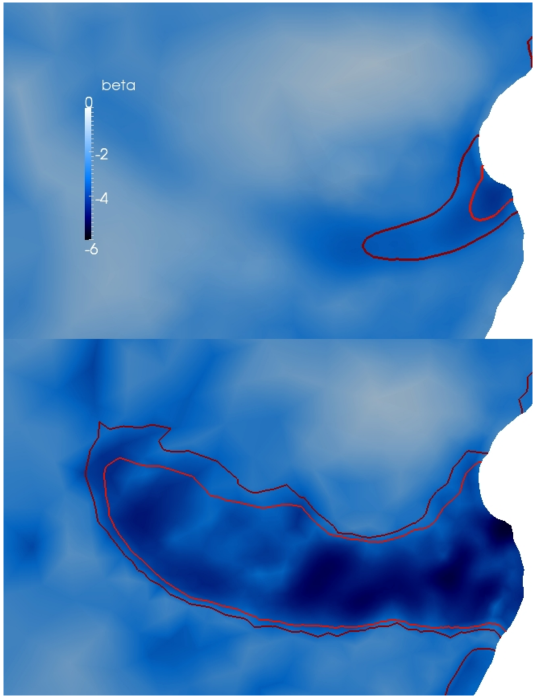

Fig. 4. Log of the basal drag coefficient, Log(β), calculated by inversion of observed surface velocities for 1995 (top panel) and 2011 (bottom panel). Units for β are $\mathrm{MPa\,a\,m^{-1}}$. Surface ice flow speed contours of 50 and $100\,\mathrm{m\,a^{-1}}$ are shown.

TCD
7, 5823–5851, 2013

Surging Svalbard glacier

R. Gladstone et al.

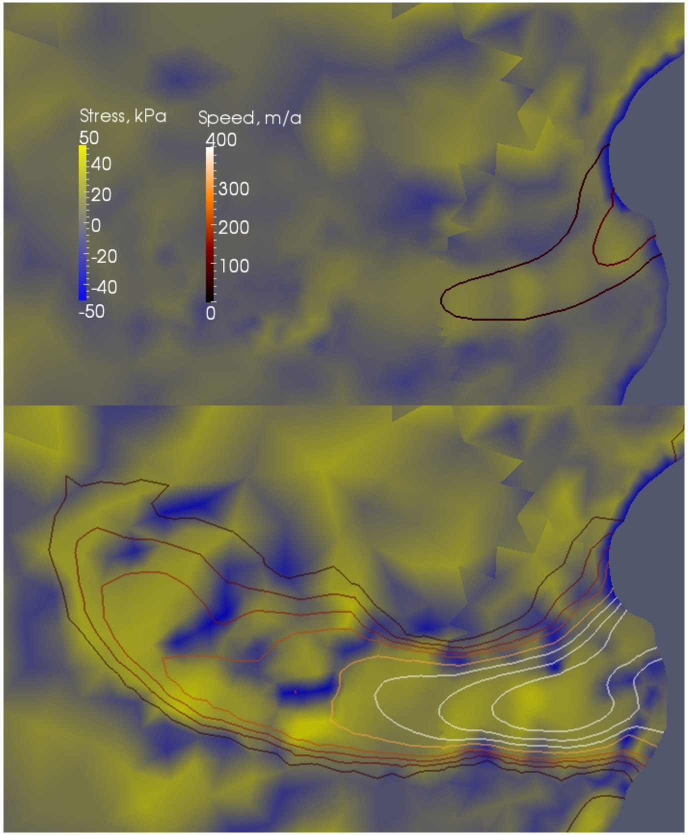

Fig. 5. Gravitational driving stress minus basal shear stress (τ_b) for 1995 (top panel) and 2011 (bottom panel), overlain by contours of surface speed. Note that the zig zag discontinuities visible in Fig. 5 are artefacts of the parallel domain decomposition in a post processing step and do not significantly affect the stress patterns.

TCD
7, 5823–5851, 2013

Title Page
Abstract Introduction
Conclusions References
Tables Figures
Back Close
Full Screen / Esc
Printer-friendly Version
Interactive Discussion

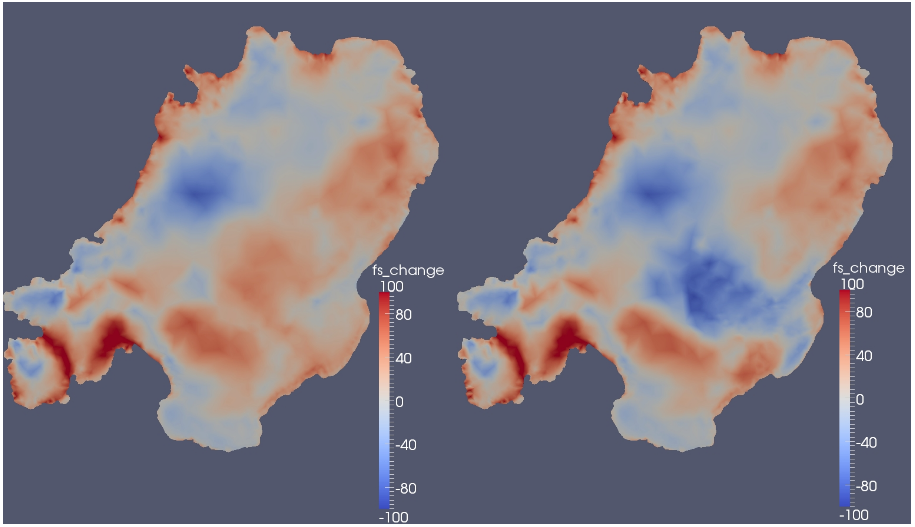

Fig. 6. Change in free surface (in m) over 100 model years using the 1995 derived basal drag field (left) and the 2011 derived basal drag field (right). The large (more than 1 $\mathrm{m\,a^{-1}}$) localised changes in South West ASF may be due to the paucity of bedrock data.

TCD
7, 5823–5851, 2013

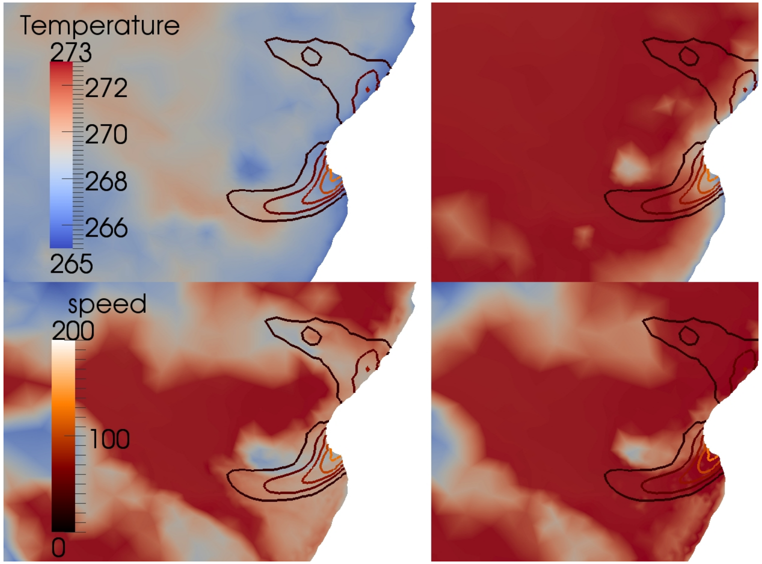

Fig. 7. ASF basal temperatures (in K) from steady state simulations. Top left: diffusion only, geothermal heat flux halved (SSLG). Top right: diffusion only (SS). Bottom left: full thermodynamics except friction heating is omitted (SS95NF). Bottom right: full thermodynamics (SS95). 1995 velocity contours (in $\mathrm{m\,a^{-1}}$) are overlain to indicate regions of fast flow.

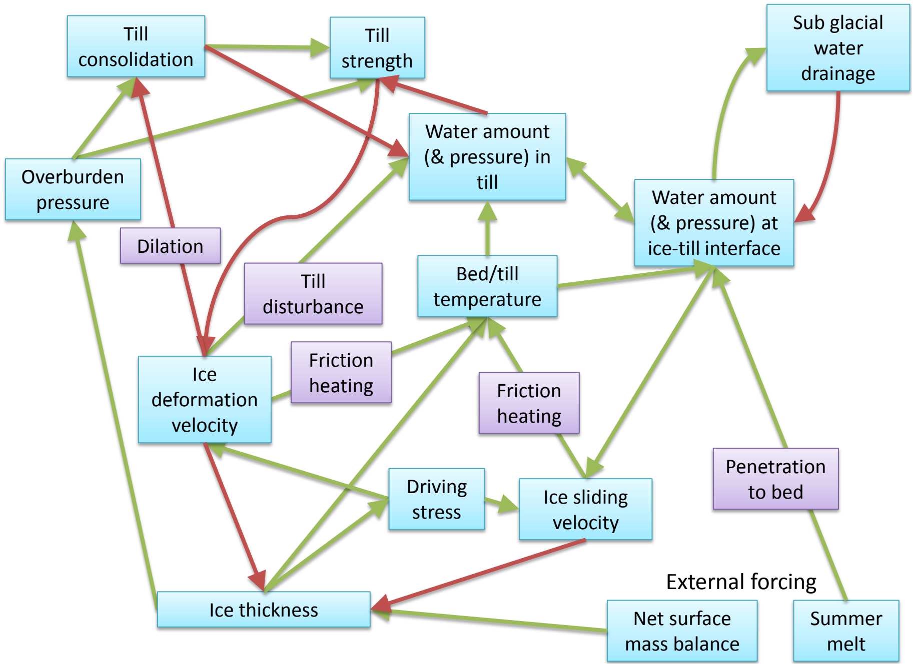

Fig. 8. Properties (blue boxes) and processes (purple boxes) at the bed, and potential relationships/feedbacks between them. Red arrows indicate an decrease in the target property and green arrows indicate an increase. So a closed loop of arrows with an odd number of red arrows indicates a negative feedback, whereas a closed loop with an even number of (or zero) red arrows indicates a positive feedback. Note the "dilation" process could change to compression depending on the state of the till, changing the sign of the feedback.